The RHIC Project — Design, Status, Challenges, and Perspectives

JIE WEI and MICHAEL HARRISON

Brookhaven National Laboratory, Upton, New York 11973, USA

The design and construction status of the Relativistic Heavy Ion Collider, RHIC, is discussed. Those novel features of a heavy ion Collider that are distinct from conventional hadron Colliders in general are noted. These features are derived from the experimental requirements of operation with a variety of ion species over a wide energy range including collisions between ions of unequal energies. The project is in the fifth year of a seven-year construction cycle. A review of the superconducting magnet program is given together with progress to date on the machine construction and commissioning. Emphasis is made on challenging issues including intrabeam scattering, interaction-region error compensation, magnet alignments, and matched transition-energy jump.

1 Introduction

The primary motivation for colliding heavy ions at ultra-relativistic energies is the belief that it is possible to create macroscopic volumes of nuclear matter at such extreme conditions of temperature and energy density that a phase transition will occur from hadronic matter to a confined plasma of quarks and gluons. The main goal of the Relativistic Heavy Ion Collider (RHIC)[1,2] is to provide head-on collisions at energies up to 100 GeV/u per beam for very heavy ions, which is defined to be gold ($^{197}Au^{79+}$), but the program also calls for lighter ions all the way down to protons and polarized protons. Luminosity requirements for the heaviest ions are specified to be in the 10^{26-27} cm^{-2}s^{-1} range. The higher Au-Au total cross-section results in interaction rates comparable to p-p Colliders although this luminosity is several orders of magnitude lower than those machines. A short interaction point (IP) length (< 20 cm rms) is desirable for optimum detector design. The final, though most influential, experiment requirement has been the need for collisions of different ion species (most notably p-Au) at the same center of mass energies per nucleon. This necessitates accommodating mass-to-charge ratios (A/Z) in the range of 1 (p) to 2.5 (Au). Stabilizing the collision point involves equalizing the rotation frequencies of the two beams, which also requires the two rings to operate at different magnetic fields. The complications in the interaction region (IR) where the beams must pass through common magnets dictate a lattice design different from conventional hadron Colliders.

Based on these general requirements, the detailed RHIC machine parameters were derived and are outlined in Table 1. Operation of the RHIC Collider at relatively low energies together with the enhanced intrabeam scattering (IBS), which scales as Z^4/A^2, results in beams of large transverse and longitudinal dimensions. This in turn has ramifications for the lattice (short cells, strong focusing) and magnet aperture. The rf system requirements are also determined by this consideration and the short IP length. Colliders, unlike fixed target machines, are designed to operate for extended periods at high energies. The economics of power consumption argue strongly for superconducting magnets. RHIC is such a superconducting machine.

Table 1: Major Parameters for the Collider.

Kinetic Ener., Inj.-Top, Au	10.8-100	GeV/u
(each beam), protons	28.3-250	GeV
No. of bunches/ring	57	
Circumference	3833.845	m
Number of crossing points	6	
β^*, injection, H/V	10	m
β^*, low-beta insertion, H/V	1	m
Betatron tunes, H/V	28.18/29.18	
Transition energy, γ_T	23.60	
Magnetic rigidity, injection	97.5	T·m
top energy	839.5	T·m
Bending radius, arc dipole	242.781	m
No. of dipoles	396	
(192/ring + 12 common)		
No. of quadrupoles	492	
(276 arc + 216 insertion)		
Dipole field at 100 GeV/u, Au	3.45	T
Arc dipole effective length	9.45	m
Arc quadrupole gradient	71.2	T/m
Arc quadrupole effective length	1.11	m
Coil i.d. arc magnets	8	cm
Coil i.d. triplet magnets	13	cm

RHIC is now in its fifth year of a seven-year construction period at the Brookhaven National Laboratory. This paper presents the design concepts, construction status, physical and technical challenges, and perspectives of the project. Fig. 1 shows a schematic layout of the collider and its existing injector complex. In Section 2, the machine design and layout is summarized. A review of the superconducting magnet program is given in Section 3. Physical and technical challenges to the design and construction is discussed in Section 4. Section 5 presents the construction status and beam test results of the AGS-to-RHIC (ATR) transfer line and the RHIC sextant. The conclusion is given in Section 6.

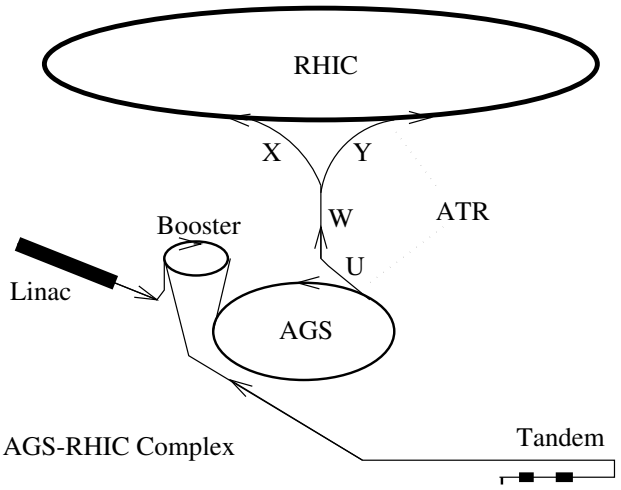

Figure 1: Schematic layout of the RHIC and the injector complex.

2 Machine Design and Layout

The complete RHIC facility is a complex set of accelerators interconnected by beam transfer lines. The collider, shown schematically in Fig. 2, is located in the existing

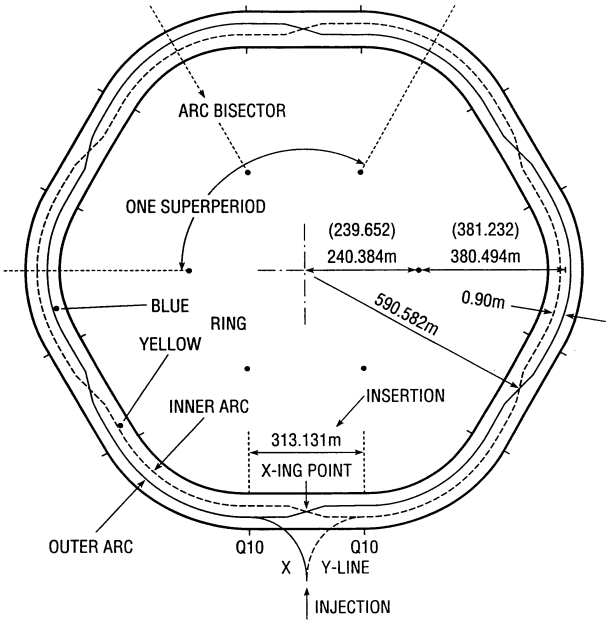

Figure 2: Layout of the Collider and the tunnel.

3.8 km tunnel north of the AGS. It is comprised of two identical, quasi-circular rings separated horizontally by 90 cm, and oriented to intersect with one another at six locations. Having a 3-fold symmetry, each ring consists of three inner and three outer arcs and six insertion regions joining them. Each arc consists of 11 FODO cells, with each half cell consisting of a single dipole and a spool-piece assembly containing a quadrupole, sextupole, and concentric correction elements. The nominal design magnetic rigidity of the dipoles is 840 T·m which corresponds to a design field of 3.45 T at 100 GeV/u. Injection takes place at 97.5 T·m. The half-cell length of 15 m has β-functions in the range from 10.5 m to 50 m, and a dispersion from 0.8 m to 1.8 m. These relatively small values are dictated by the need to minimize the physical size of a beam (i.e. maximize dynamic aperture and thus intensity lifetime) with relatively large emittances (40π mm·mr normalized 95% transverse, 1.2 eV·s/u longitudinal). The dipole coil inner diameter (i.d.) of 8 cm is determined both by the beam size at injection and by the projected emittance growth which occurs during a store at the lowest collision energy of 30 GeV/u. The quadrupoles, also having a coil i.d. of 8 cm, operate at a maximum gradient of 72 T/m. A cross-section of a dipole of length 9.45 m is shown in Fig. 3. The mag-

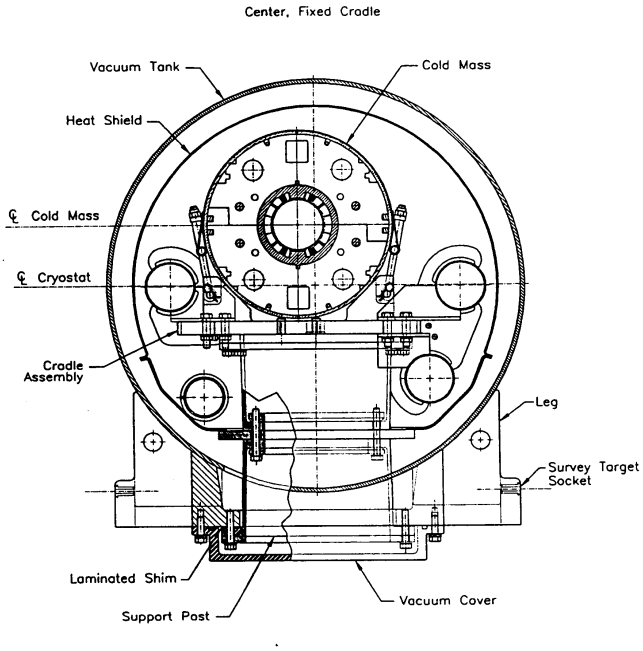

Figure 3: Arc dipole with cryostat cross section.

nets are conceptually similar to the HERA dipoles with a "cold-iron" design and cryogenic transfer lines located in the cryostat.

Collisions of the beams take place at the crossing point of the insertions. These regions contain the optics necessary for producing small betatron amplitude functions $\beta^*_{x,y}$ and a zero dispersion at the crossing point, and the magnet bending to bring the beams into head-on collisions. The "non-arc" regions also contain the only warm regions of the machine where the machine utilities reside such as injection, beam abort, rf station, collimators, and specialized instrumentation. Locations available for these devices are the 35 m section between Q3

and Q4, the missing dipole between Q7 and Q8, and the section adjacent to the short D9 dipole. The magnetic elements in the region from Q10 to Q4 are identical in cross-section but different in length to those in the standard cell. The final focus triplet (Q1, Q2, and Q3), and bending magnets (D0 and DX) are non-standard magnets with apertures of 13 cm, 10 cm, and 18 cm, respectively. The focusing is relaxed at injection with a β^* value of 10 m. During collisions at top energy, a β^* of 1 m can be attained resulting a maximum β of about 1400 m in the triplet quadrupoles. The maximum focusing strength of about 48 T/m is determined by both the physical beam size in the triplet and the strength of the trim quadrupoles at Q4, Q5, and Q6. The lattice functions in the IR's are shown in Fig. 4. Each insertion is

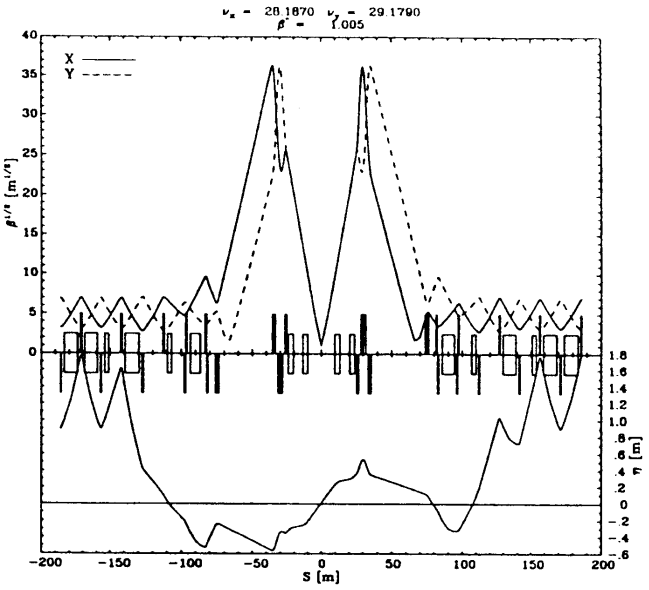

Figure 4: Betatron and dispersion functions in the insertion region.

independently adjustable and can be matched over a machine tune range of ± 1 unit. The phase advance across the insertion is almost constant during the squeeze, as is the triplet excitation.

3 Magnet Program

A major goal of the project to date has been the superconducting magnet construction program. The magnets naturally fall into two types; the 8 cm elements which are used throughout the arc regions and constitute the bulk of the magnets, and the smaller number of variable aperture magnets used in the immediate vicinity of the IP. A list of the various magnet type is given in Table 2.

The 8 cm dipoles, quadrupoles, and sextupoles were all produced industrially. The low-current correctors,

Table 2: RHIC magnet inventory.

Magnet	Needed	Spare
8 cm dipoles	360	10
8 cm quadrupoles	420	12
trim quadrupoles	72	6
sextupoles	288	12
8 cm multilayer correctors	420	10
13 cm IR quadrupoles	72	6
13 cm IR correctors	72	6
10 cm IR dipoles	24	2
18 cm IR dipoles	12	1

final-focus triplet quadrupoles and beam splitting dipoles were produced internally by BNL. BNL also performed the integration of the quadrupoles, sextupoles, and correctors into a single cryogenic module. The dipole magnets, produced by the Northrop-Grumman Corporation in a build-to-print contract, were complete cryogenic elements suitable for immediate installation. The industrially produced magnets were completed during a two year period from 1994 to 1996. The BNL production program will continue through 1998.

The crucial aspects of superconducting accelerator magnets involve field quality and quench threshold.[3] Since it was decided that cold testing of each magnet was not realistic, it became important to establish that there was a good correlation between warm and cold magnetic field measurements. An analysis of the complete data set demonstrated that after compensating for yoke saturation effects, good warm/cold field correlations can be obtained. The distribution of field harmonics for the full set of dipole magnets is shown in Fig. 5. The magnet set demonstrates excellent field quality with very small random multipole field components by virtue of tight mechanical tolerances on the cable dimensions.[4] The systematic component of the field harmonics is optimized for low-field performance at injection with yoke saturation apparent in the allowed harmonics at high field. During collisions the dynamic aperture is determined by the triplet quadrupoles[5,6] with a maximum β of 1400 m. Special techniques used for triplet construction will be discussed in Section 4.

The quench performance of the 8 cm dipole magnets is shown in Fig. 6 with the minimum and plateau quench currents for a set of 60 magnets. Since only 20% of the magnets are measured cold, it is important to demonstrate sufficient operating margin to make limited testing viable. None of the magnets tested to date have had an initial quench current less than the nominal operating level. The plateau quench level demonstrates a healthy 30% operating margin. For the smaller number of IR magnets with less predicted margin, all of them will be cold tested in a vertical dewar.

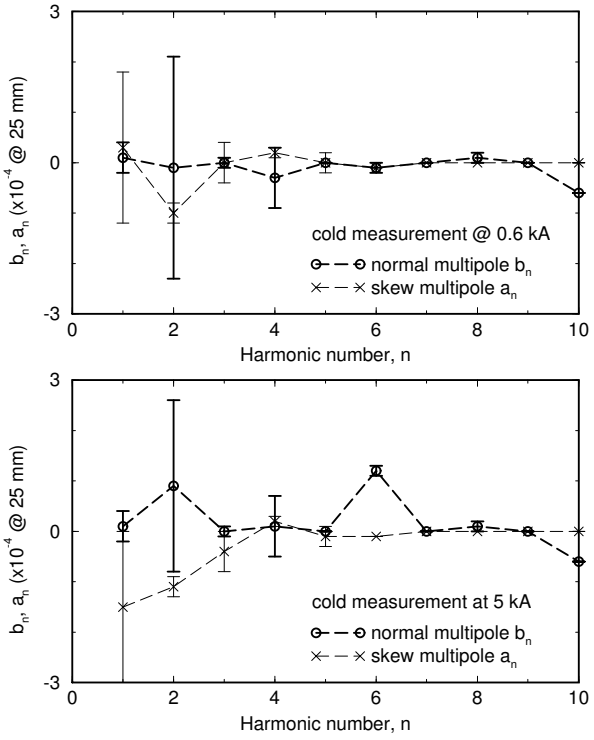

Figure 5: Arc dipole magnetic field multipole harmonics at injection (0.6 kA) and storage (5 kA) currents.

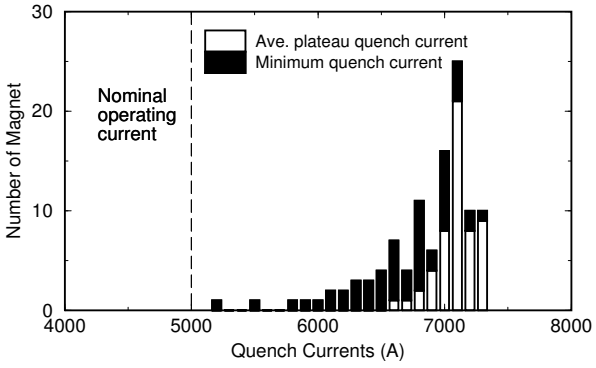

Figure 6: Dipole magnet quench current distribution.

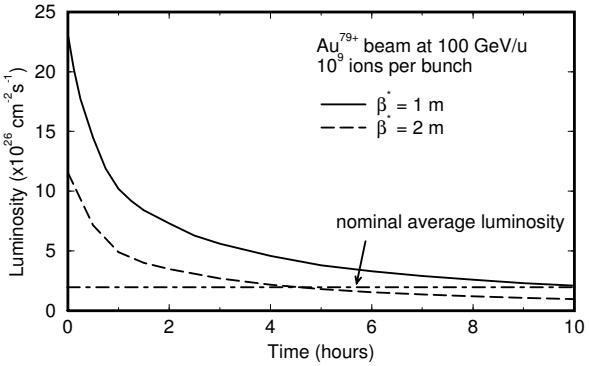

Figure 7: Luminosity reduction caused by intrabeam scattering during a 10-hour store for a crossing point with a β^* of 1 m and 2 m, respectively.

4 Physical and Technical Challenges

4.1 Intrabeam Scattering

Beam growth caused by intrabeam scattering[7] is of primary concern during the injection and store of the heavy ion beams. At injection, the IBS growth time of the momentum spread is about 3 minutes. Alternate filling of the two rings, each with 57 bunches, needs to be done within about 1 minute to prevent difficulty in transition crossing and top-energy rf recapture due to increased longitudinal beam size. At storage, emittance growth occurs in both transverse and longitudinal dimension with e-folding rates given by

$$\tau_p^{-1} \sim \tau_x^{-1} \sim 34.6 L_c r_0^2 E_0 \frac{Z^4 N}{A^2 \gamma_T \epsilon_x \epsilon_y S}, \qquad (1)$$

where N is the number of ions per bunch, ϵ_x, ϵ_y, and S are the 95% normalized transverse emittances and bunch area, $E_0 = 0.931$ GeV, $r_0 \approx 1.53 \times 10^{-18}$ m, and $L_c \approx 20$ is the Coulomb logarithm. Fig. 7 shows the luminosity reduction caused by IBS emittance growth and beam loss during a 10-hour store. Transverse emittances grow from the initial 10π mm·mr to more than 40π mm·mr. Longitudinal bunch area exceeds the bucket area of 1.2 eV·s/u in about an hour. Collimation systems are designed to remove particles escaped from the rf buckets. Increasing peak rf voltage only modestly improves the luminosity performance, since transverse growth is significant, and since momentum aperture can be a limitation. The ultimate improvement can be made if cooling methods are adopted. Fig. 8 shows the improvement of integrated luminosity over a 10-hour store if transverse and longitudinal stochastic cooling[8] are employed to counter-act intrabeam scattering.

4.2 IR Error Compensation

In order to maximize the luminosity at two IPs with proposed experiments, their nearby triplets are designed to enable the collision β^* to be reduced to $\beta^* = 1$ m. Dipoles and triplets of quadrupoles of large bore are placed on both sides of the IP. The peaked β of 1400 m, along with the strong IBS growth, makes the 5σ beam size to increases from 35% to about 70% of the triplet magnet coil radius. In order to optimize the field quality in these elements, some of the most advanced and sophisticated compensation techniques are developed,[5] including individual error correction with tuning shims, ampli-

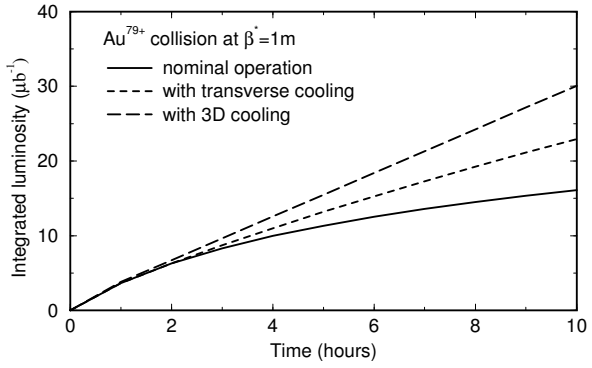

Figure 8: Integrated luminosities during a 10-hour store for a) the nominal operation (without cooling), b) with transverse stochastic cooling, and c) with both transverse and longitudinal stochastic cooling. The bandwidth of the cooling system is assumed to be 4–8 GHz.

tude dependent body-ends compensation, low-β^* sorting, and lumped triplet multi-layer corrector packages, as shown in Fig. 9 and outlined in Table 3. As shown

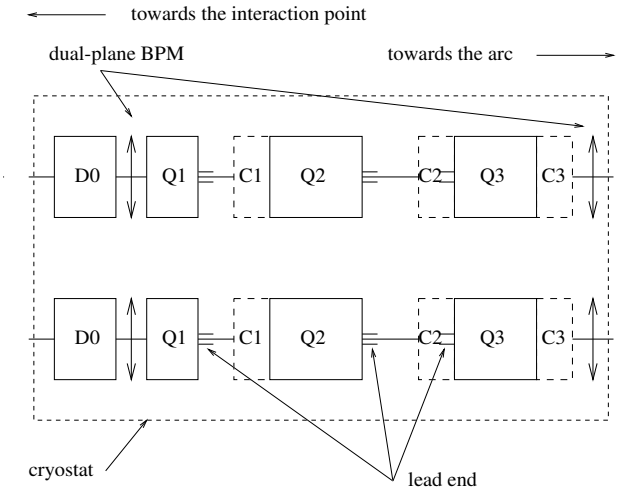

Figure 9: Schematic layout of the RHIC triplet cryostat assembly, showing the dipoles (D0), quadrupoles (Q1, Q2, and Q3) and their lead-end orientation, triplet correctors (C1, C2, and C3), and dual-plane BPMs of both rings.

in Fig. 10, tuning shims are planned to be inserted into the 8 empty slots of the IR quadrupole body to compensate the lower eight harmonics[9] after the magnet is constructed and individually warm measured. Recent experiments indicate that leading multipole errors can be reduced to about 10% rms of the uncorrected value. Table 4 shows the expected and measured multipole harmonics after tuning shims are inserted. The expected values for the mean and its uncertainty often become zero, and the standard deviation is associated with a roll up of measurement errors, thermal cycling fluctuations, and quench fluctuations. The non-zero targeted $\langle b_5 \rangle$ and

Table 3: The IR triplet correction strategy.

Order, n	Normal, b_n	Skew, a_n
0	C1 or C3	C3 or C1
1	individually powered	C2
2	S, C3	S, C2
3	B, S, C1, C3	S, C2
4	S, C1	S
5	B+, S+, C1, C3	S+, C2
7	B	
9	B	

B: coil cross-section iteration
B+: cross-section iteration plus body-ends compensation
S: using tuning shims
S+: tuning shims on random b_5/a_5 after body-ends compensation on systematic b_5/a_5.
C1, C2, C3: correction available at C1, C2, or C3 corrector

$\langle a_5 \rangle$ are results of amplitude-dependent compensation.

Lumped correctors located in the triplet region are used to correct closed-orbit errors, to perform local decoupling, and to correct higher-order multipole errors both from dipoles (D0) and IR quadrupoles. Because the β-function varies rapidly from body to end in the triplet, higher-order multipole corrections in both horizontal and vertical directions can be best achieved with two correctors in the triplet, which are located at places with significantly different β_x/β_y ratio. As shown in Table 3, the b_3 and b_5 correctors are designed to compensate for the residual errors in the quadrupoles after shimming and for D0 cross coupling. All the skew correctors a_1, a_2, a_3, and a_5 are located at C2, where β_x and β_y are about equal. Except for dipole (b_0/a_0) and skew quadrupole (a_1), all of these correctors are planned to be dead reckoned to correct the measured construction error. The a_1 correctors, totally 12 per ring, are planned to be used[10] along with the dual-plane BPMs for local decoupling.

4.3 Magnet Alignments

An accurate alignment of the arc corrector-quadrupole-sextupole (CQS) assembly[11] is crucial for the polarized proton operation. An accurate alignment of the triplet assembly is crucial for the low-β^* heavy ion operation. The critical issue in the alignment is to accurately locate the magnetic centers and rolls of the cold masses after they are fully assembled. In early CQSs, a colloidal-cell[12] technique was used to locate the transverse quadrupole field center with respect to the external fiducials. In recent CQSs and triplets, a magnetic antenna technique is used to locate the centers of quadrupoles, sextupoles, and multi-layer correctors. The measurement is done at

Table 4: Expected values of the mean ($\langle b_n \rangle$, $\langle a_n \rangle$), uncertainty in mean ($d(b_n)$, $d(a_n)$), and standard deviation ($\sigma(b_n)$, $\sigma(a_n)$) of the integral, lead end, and return end harmonics of the triplet quadrupole Q1 at storage current (5 kA) with nominal tuning shims inserted. The integral harmonics are expressed in 10^{-4} of the quadrupole integral strength at the reference radius of 40 mm. The lead-end and return-end harmonics are expressed in an integrated form in unit-meters.

Order, n	Normal					Skew				
	Expected			Measured		Expected			Measured	
Integral (unit)	$\langle b_n \rangle$	$d(b_n)$	$\sigma(b_n)$	$\langle b_n \rangle$	$\sigma(b_n)$	$\langle a_n \rangle$	$d(a_n)$	$\sigma(a_n)$	$\langle a_n \rangle$	$\sigma(a_n)$
1	0.0	0.0	0.0	0.0	0.0	0.0	0.0	10.0	0.0	0.0
2	0.0	0.0	0.5	0.3	0.5	0.0	0.0	0.5	0.5	0.2
3	0.0	0.0	0.4	0.4	0.4	0.0	0.0	0.4	−0.3	0.4
4	0.0	0.0	0.3	0.1	0.3	0.0	0.0	0.3	−0.1	0.3
5	2.7	0.0	0.2	2.6	0.2	0.0	0.0	0.2	−0.6	0.2
6	0.0	0.1	0.1	−0.0	0.1	0.0	0.1	0.1	0.3	0.3
7	−0.2	0.05	0.05	−0.3	0.3	0.0	0.03	0.1	−0.0	0.0
8	0.0	0.04	0.05	−0.0	0.0	0.0	0.05	0.1	0.0	0.1
9	0.0	0.2	0.03	−0.1	0.4	0.0	0.03	0.03	0.2	0.0
Lead end (unit·m)	$\langle B_n \rangle$	$d(B_n)$	$\sigma(B_n)$	$\langle B_n \rangle$	$\sigma(B_n)$	$\langle A_n \rangle$	$d(A_n)$	$\sigma(A_n)$	$\langle A_n \rangle$	$\sigma(A_n)$
1	0.0	0.0	0.0	0.0	0.0	0.0	0.0	0.0	0.0	0.0
2	0.0	0.1	0.7	0.1	0.9	0.0	1.0	2.0	0.8	1.2
3	0.0	0.3	0.3	−0.1	0.1	0.0	0.4	0.8	−0.9	0.4
4	0.0	0.1	0.3	−0.1	0.4	0.0	0.3	0.4	0.5	0.5
5	4.6	0.5	0.3	4.6	0.2	−1.5	0.5	0.2	−1.4	0.1
7	0.0	0.04	0.05	0.0	0.0	0.0	0.02	0.01	−0.0	0.0
9	−0.5	0.05	0.02	−0.5	0.0	0.2	0.05	0.03	0.2	0.0
Return end (unit·m)	$\langle B_n \rangle$	$d(B_n)$	$\sigma(B_n)$	$\langle B_n \rangle$	$\sigma(B_n)$	$\langle A_n \rangle$	$d(A_n)$	$\sigma(A_n)$	$\langle A_n \rangle$	$\sigma(A_n)$
1	0.0	0.0	0.0	0.0	0.0	0.0	0.0	0.0	0.0	0.0
2	0.0	0.3	1.8	−0.1	0.4	0.0	0.7	1.0	−0.1	0.5
3	0.0	0.1	0.2	−0.2	0.3	0.0	0.1	0.3	0.4	0.3
4	0.0	0.0	0.25	−0.1	0.4	0.0	0.2	0.2	0.2	0.2
5	1.0	0.0	0.6	0.5	0.3	0.0	0.1	0.1	−0.1	0.2
7	0.0	0.01	0.02	0.0	0.0	0.0	0.02	0.05	0.0	0.1
9	−0.1	0.0	0.03	−0.1	0.0	0.0	0.04	0.01	0.0	0.0

several locations along the longitudinal axis with an estimated error of from 0.05 to 0.1 mm. Choreographed welding is used to balance distortion and to minimize offsets.

4.4 Transition Crossing

RHIC will be the first superconducting accelerator to cross transition energy. Due to the slow ramping rate of the superconducting magnets, both chromatic nonlinear effects and beam self-field effects are strong at crossing.[13] A "matched first order" transition jump scheme is designed[14] to effectively increase the crossing rate by a factor of 8 during the 60 ms time around transition. With such a scheme, Fig. 12 shows that longitudinal emittance growth can be limited to less than 20% at transition with minimum disruption to the transverse particle motion.

5 Construction and Commissioning Status

5.1 Ring Installation

With the delivery to the tunnel of over 600 cryogenic magnets, installation activities are proceed at full speed. All of the magnets are in place for the arc sections, and magnet interfacing has started on these regions. Joining two magnets together requires 7 pipe connections together with heat shields, instrumentation leads, vacuum ports, and super insulation. The present rate of 1 interconnect per day will be doubled shortly which will result in all the 8 cm magnets installed by the spring of 1998.

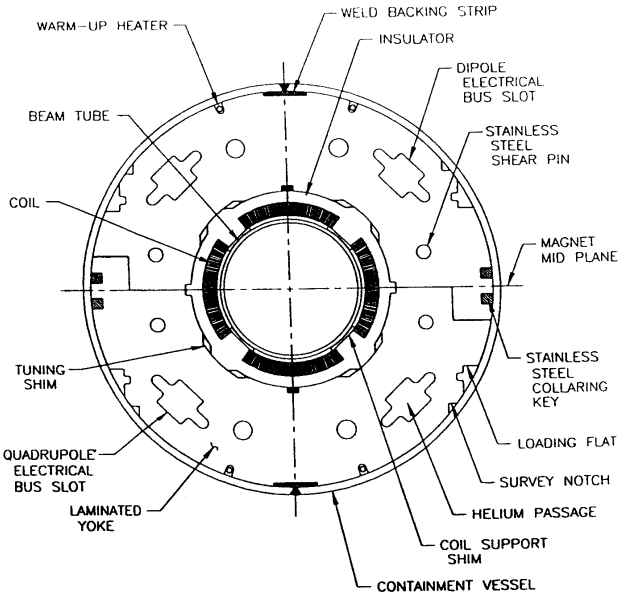

Figure 10: Triplet quadrupole cross-section showing empty slots for tuning shims.

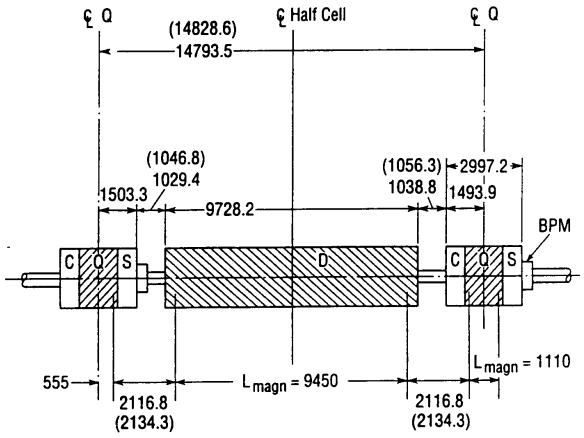

Figure 11: Schematic layout of the CQS assembly.

The first sextant of the machine including the interaction region quadrupole triplets and beam separating dipoles have been constructed. The lateral separation in this region requires that two cold masses are in a single cryostat. The physical size of this cryostat necessitates that it be constructed *in situ* with the magnets transported to the tunnel as cold masses. In addition to magnet installation, work is proceeding on other systems. Cryogenic distribution piping is a significant effort. The connection between the central refrigerator and the tunnel, and the first sextant, has been completed. The main 5 KA power supplies are installed and the first of the superconducting buss connecting to the magnets is in place.

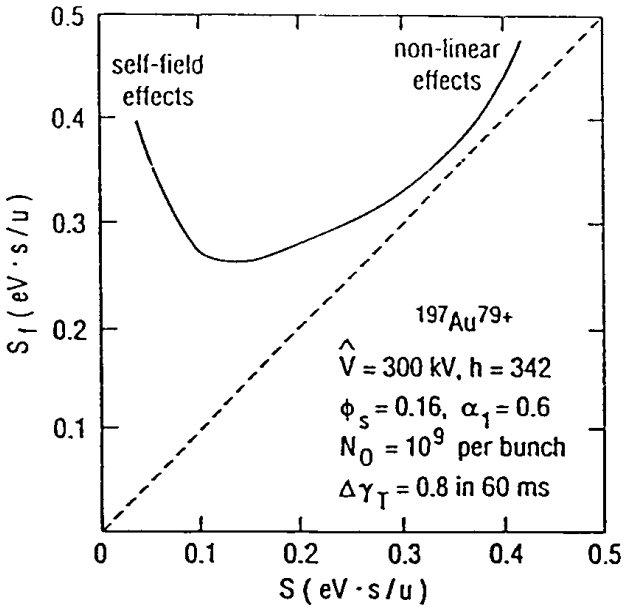

Figure 12: Effects of chromatic nonlinearities and self fields at transition.

5.2 ATR Test

The beam extraction system from the AGS and the injection line was completed during the summer of 1995. Several months later, gold beam was transported down the line to an internal beam dump.[15] This was the first of a series of integrated systems tests planned for the project. The first step in this test required the commissioning of a new AGS fast extraction system and was operated in a parasitic "cycle stealing" mode during normal AGS heavy ion operations. The injection line was the first demonstration of several of the final designed RHIC systems: controls, vacuum, instrumentation, and power supplies. Measurements were made of the beam line optics and beam parameters and revealed good agreement with the nominal design parameters.[16] Fig. 13 shows a comparison on dispersion between the design and measurement obtained by evaluating beam centroid positions on Beam Position Monitors and Beam Profile Monitors as a function of beam radial orbit in the AGS.

5.3 Sextant Test

Starting early 1997, a major test of the accelerator systems has been under way for the completed sextant of the machine. The first step has been a cooldown and powering of the elements. Subsequently, beam was transported through the magnet string to the sextant internal dump. This test required a subset of essentially all of the different accelerator components and was a significant step in validating the machine hardware designs. Attempts have been made to commission the first application soft-

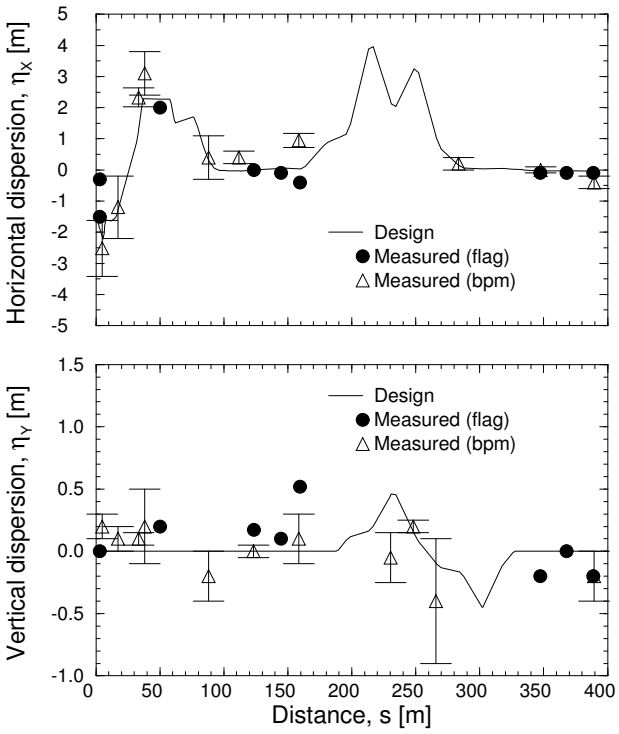

Figure 13: Dispersion function of the ATR measured by varying the AGS beam momentum.

ware with low level rf beam synchronization, ramping, and storage. Beam physics studies included measurements of machine properties (difference orbits, momentum aperture, dispersion, phase advance, chromaticity, etc.), beam parameters (energy, intensity, transverse and longitudinal emittances) and system stabilities (hysteresis, system noise, etc.). As an example, Fig. 14 shows a good agreement on horizontal phase advance of the sextant arc as a function of focusing quadrupole strength between MAD lattice modelling and beam measurement, which was obtained by measuring beam centroid positions on the sextant Beam Profile Monitor while sequentially varying the sextant dipole corrector strength.

6 Conclusions

Although a significant amount of work remains to be done, the RHIC project is on track to start commissioning at the beginning of 1999. The machine design is stable and the component installation is in full swing. Current major systems tests has been used to exercise the accelerator components. Commissioning and beam test of both AGS-to-RHIC transfer line and the first RHIC sextant has been successful.

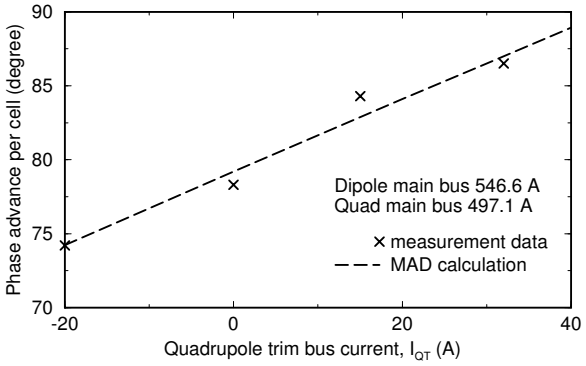

Figure 14: Comparison between the measurement and MAD lattice modelling on horizontal phase advance per cell as a function of arc focusing quadrupole strength.

Acknowledgments

Work performed under the auspice of the U.S. Department of Energy.

References

1. *RHIC Design Manual* (Brookhaven National Laboratory, Upton, 1996).
2. M. Harrison, *The RHIC Project*, Proc. 5th Euro. Part. Accel. Conf., Sitges, 13 (1996).
3. J. Wei, R.C. Gupta, A. Jain, S.G. Peggs, C.G. Trahern, D. Trbojevic, P. Wanderer, *Field Quality Evaluation of the Superconducting Magnets for the Relativistic Heavy Ion Collider*, Proc. 1995 Part. Accel. Conf. and Inter. Conf. on High-Energy Accel., Dallas (1995) 461.
4. S. Peggs, *Feedback between Accelerator Physicists and Magnet Builders*, Particle Accelerators, **55** 83, 1996.
5. J. Wei, *Error Compensation in Insertion-Region Magnets*, Particle Accelerators, **55** 439–448, 1996.
6. J. Wei, R. Gupta, and S. Peggs, *Magnet Correction of RHIC Triplets*, Proc. 1993 Part. Accel. Conf., Washington, D.C., (1993), p. 257.
7. J. Wei, *Evolution of Hadron Beams under Intrabeam Scattering*, Proc. 1993 Part. Accel. Conf., Washington, D.C. (1993) p.3653.
8. J. Wei, *Stochastic Cooling and Intra-Beam Scattering in RHIC*, Proc. Workshop on Beam Cooling and Related Topics, Montreux, p.132, 1994 (CERN 94-03).
9. R. Gupta, *Estimating and Adjusting Field Quality in Superconducting Magnets*, Particle Accelerators, **55** 375, 1996.
10. F. Pilat, S. Peggs, S. Tepikian, D. Trbojevic, J. Wei, *The Effect and Correction of Coupling Gener-*

ated by the RHIC Triplet Quadrupoles, Proc. 1995 Part. Accel. Conf., Dallas, 2832 (1995).
11. J. Wei, G. Ganetis, R. Gupta, M. Harrison, M. Hemmer, A. Jain, F. Karl, S. Peggs, S. Tepikian, P.A. Thompson, D. Trbojevic, P. Wanderer, *Misalignment Evaluation of Superconducting Magnets in the Relativistic Heavy Ion Collider*, Proc. 5th Euro. Part. Accel. Conf., Sitges, 2222 (1996).
12. D. Trbojevic, P. Cameron, et. al., *Alignment and Survey Elements in RHIC*, Proc. 1995 Part. Accel. Confe., Dallas, 2099 (1995).
13. J. Wei, *Longitudinal Dynamics of the Non-Adiabatic Regime on Alternating-Gradient Synchrotrons*, Ph. D. dissertation, Stony Brook, New York (1990); revised 1994.
14. S. Peggs, S. Tepikian, D. Trbojevic, *A First Order Transition Jump at RHIC*, Proc. 1993 Part. Accel. Conf., (Washington D.C., 1993), p.168.
15. W.W. MacKay, et.al., *AGS to RHIC Transfer Line: Design and Commissioning*, Proc. 5th Euro. Part. Accel. Conf., Sitges, 2376 (1996).
16. T. Satogata, et.al., *Physics During the 1995 AGS-to-RHIC Transfer Line Commissioning*, Proc. 5th Euro. Part. Accel. Conf., Sitges, 2379 (1996).